Taylor & Francis
Taylor & Francis Group

Journal of Maps

ISSN: (Print) (Online) Journal homepage: https://www.tandfonline.com/loi/tjom20

Geomorphology of the upper sector of the Roncovetro active landslide (Emilia-Romagna Region, Italy)

Giulia Dotta, Alessandro Fornaciai, Giovanni Bertolini, Iaria Isola, Luca Nannipieri, Massimiliano Favalli, Pierfrancesco Burrato, Roberto Devoti, Giovanni Gigli, Lorenzo Mucchi, Emanuele Intrieri, Marco Pizziolo, Teresa Gracchi & Nicola Casagli

To cite this article: Giulia Dotta, Alessandro Fornaciai, Giovanni Bertolini, Iaria Isola, Luca Nannipieri, Massimiliano Favalli, Pierfrancesco Burrato, Roberto Devoti, Giovanni Gigli, Lorenzo Mucchi, Emanuele Intrieri, Marco Pizziolo, Teresa Gracchi & Nicola Casagli (2023) Geomorphology of the upper sector of the Roncovetro active landslide (Emilia-Romagna Region, Italy), Journal of Maps, 19:1, 1-11, DOI: 10.1080/17445647.2023.2277898

To link to this article: https://doi.org/10.1080/17445647.2023.2277898

Published online: 21 Nov 2023.

JOURNAL OF MAPS
2023, VOL. 19, NO. 1, 2277898
https://doi.org/10.1080/17445647.2023.2277898

SCIENCE

OPEN ACCESS Check for updates

Geomorphology of the upper sector of the Roncovetro active landslide (Emilia-Romagna Region, Italy)

Giulia Dotta[a], Alessandro Fornaciai[a], Giovanni Bertolini[b], Ilaria Isola[a], Luca Nannipieri[a], Massimiliano Favalli[a], Pierfrancesco Burrato[c], Roberto Devoti[d], Giovanni Gigli[e], Lorenzo Mucchi[f], Emanuele Intrieri[e], Marco Pizziolo[g], Teresa Gracchi[e,*] and Nicola Casagli[e,h]

[a]Sezione di Pisa, Istituto Nazionale di Geofisica e Vulcanologia, Pisa, Italy; [b]Reggio Emilia Office, Emilia-Romagna Regional Agency for Territorial Security and Civil Protection, Reggio Emilia, Italy; [c]Sezione Roma 1, Istituto Nazionale di Geofisica e Vulcanologia, Rome, Italy; [d]Osservatorio Nazionale Terremoti, Istituto Nazionale di Geofisica e Vulcanologia, Rome Italy; [e]Department of Earth Sciences, Università degli Studi di Firenze, Florence, Italy; [f]Department of Information Engineering, Università degli Studi di Firenze, Florence, Italy; [g]Emilia-Romagna Regional Administration, Directorate for Territorial and Environmental Care, Bologna, Italy; [h]National Institute of Oceanography and Applied Geophysics – OGS, Trieste, Italy

ABSTRACT

We present the geomorphological map of the upper sector of the Roncovetro active landslide (Enza Valley, Emilia-Romagna, Italy). The 1:1500 scale map provides an accurate picture of the landslide in October 2014. The map is mainly based on the data collected during an airborne LiDAR survey. The capability of LiDAR to 'penetrate' the vegetation cover makes these data the most complete and accurate topographic dataset of this landslide. The map shows that the upper sector of the Roncovetro landslide consists of gravity- and water runoff-related forms. Gravitational features are linked to sliding and flowing movements that characterize the short- and long-term behaviour of the landslide. By comparing the 2014 LiDAR-Digital Elevation Model (DEM) with the 1973 DEM provided by the Emilia-Romagna Region, we calculated that $6.2 \pm 0.8 \times 10^5$ m^3 of material has moved from the top of the Roncovetro landslide in about 40 years.

ARTICLE HISTORY
Received 23 March 2023
Revised 19 October 2023
Accepted 25 October 2023

KEYWORDS
Landslides; geomorphological map; LiDAR; Digital Elevation Model (DEM); topographic change detection

1. Introduction

The Roncovetro landslide, also known as Lavina di Roncovetro (Bertolini & Gorgoni, 2001) or Vedriano landslide (Cervi & Tazioli, 2021), is a 2.5 km long complex earth flow (Cruden & Varnes, 1996) located in the Enza Valley (Municipality of Canossa, Emilia-Romagna Region, Italy) on the southern slope of Mount Staffola and extends from its top, down to the Tassobbio Stream (Figure 1). The Roncovetro landslide seriously menaced an edifice located next to its crown, as well as electric and water supply pipelines. To protect the road that once linked Vedriano and Roncovetro villages passing through the top of Monte Staffola, in the 1990s, the Emilia-Romagna Region (RER) installed imposing retaining structures on the crown. These structures are now largely damaged by the landslide movement and the road is impassable because the crown retratment. Moreover, the white road linking the villages of Roncovetro and Vedriano (Figure 1) is periodically flooded by earth flow. From 2014 till the time of writing, this road was swept away four times: in March 2015, May 2019 (Gracchi, 2019), December 2020 and March 2023.

The Roncovetro landslide is accessible in its upper part and it is easy to reach by car. It alternates phases of small movements, mainly superficial, that involve a small volume of material, with events during which a significant volume of detached materials move from the upper sector of the landslide to the channelized downslope sectors (Bertolini & Gorgoni, 2001). For these reasons, the Roncovetro landslide was chosen as a test site for assessing new monitoring technologies in the frame of the LIFE + European project (LIFE12-ENV/IT/001033) 'Wireless sensor network for Ground Instability Monitoring' (Wi-GIM; Intrieri et al., 2018; Mucchi et al., 2018), and as test site for the Project 'Integrated and multi-scale approach for the definition of earthquake-induced landslide hazard in the Italian territory' financed by the Italian Ministry of Environment, Land and Sea. At the time of writing, it was also chosen as an area of interest for the 'Landslide Enhanced Monitoring Network' project funded by Istituto Nazionale di Geofisica e Vulcanologia.

CONTACT Alessandro Fornaciai alessandro.fornaciai@ingv.it Sezione di Pisa, Istituto Nazionale di Geofisica e Vulcanologia, 56125 Pisa, Italy
Supplemental data for this article can be accessed online at https://doi.org/10.1080/17445647.2023.2277898.
*Present address: National Institute of Oceanography and Applied Geophysics – OGS, Trieste, Italy

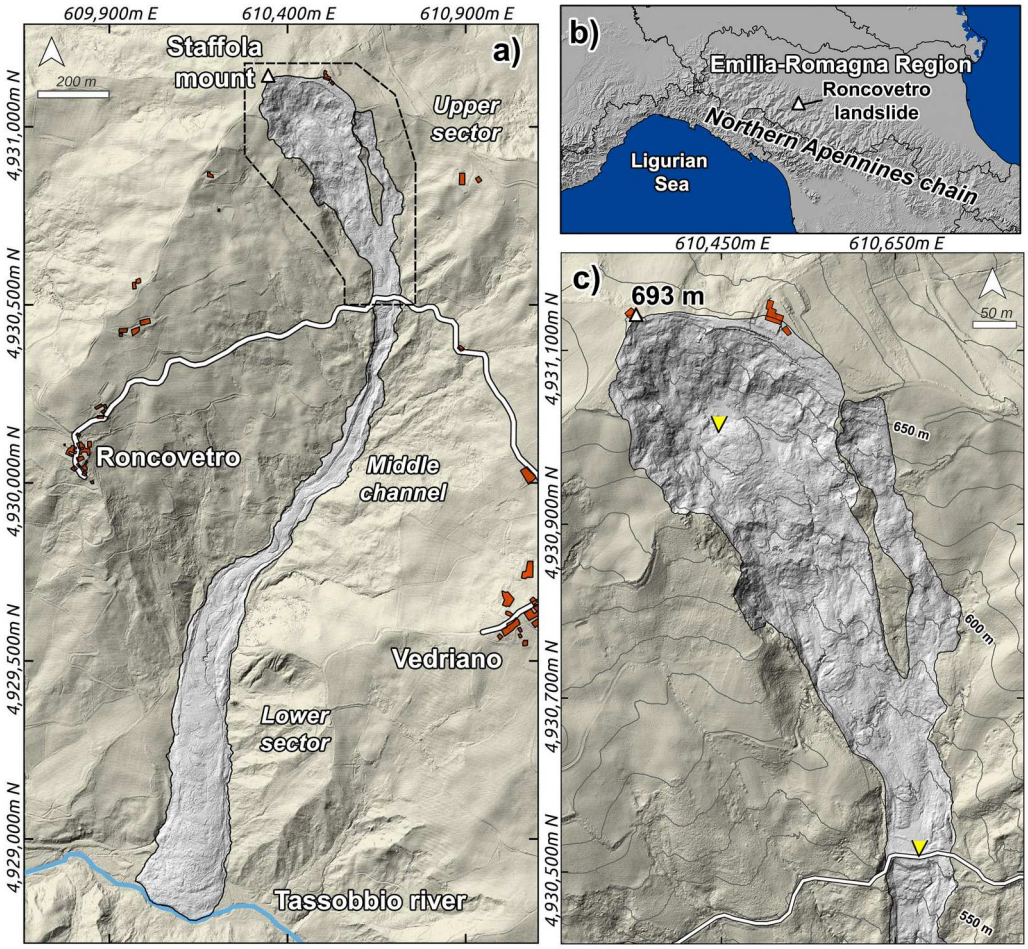

Figure 1. Location of the study area in WGS84 UTM32 coordinate reference system. (a) The Roncovetro landslide imaged by the hillshading of the 2014 Airborne LiDAR DEM. The main menaced assets were reported on the map The dotted line indicates the area of study. (b) The regional location of the Roncovetro landslide over the hillshading of the TINITALY DEM (Tarquini et al., 2012). (c) The upper sector of the Roncovetro landslide. 10 m spaced elevation lines are reported. The yellow markers indicate the snapshot positions of the photos in Figure 7(a) (the uppermost marker) and Figure 7(b) (the lowermost marker).

During these projects, field mapping and remote laser scanning surveys were carried out. In particular, during the Wi-GIM project, an airborne Light Detection And Ranging (LiDAR) survey of the landslide was realized in October 2014 (Figure 1). The LiDAR-derived Digital Elevation Model (DEM) and its derivated variables were used to analyse and map the geomorphological features of the landslide. In this work, we present the 1:1500 scale geomorphological map of the upper sector of the Roncovetro landslide (Main Map). The map shows: (i) the landslide upper limit (i.e. crown); (ii) the morphological linear elements within the landslide area (i.e. morphological scarp lines, crests, counter-slopes,transverse and crown cracks); (iii) the landforms and deposits related to gravity (i.e. main scarp, landslide body); (iv) fluvial and runoff erosional and depositional elements (i.e. rills, gullies, erosion scarps, crests, alluvial fans, ponds); (v) anthropic structures (i.e. crib walls, roads and buildings). In addition, by comparing the 2014 LiDAR DEM and 1973 RER DEMs, we calculate the volume of material mobilized on the upper sector of the landslide in about 40 years.

2. Study area

2.1. Geological and seismotectonic setting

The Roncovetro landslide falls within the NE-verging Northern Apennines (NA) fold-and-thrust belt, and it is located about 15 km at the rear of its thrust delimited mountain front. The NA evolved during the Africa-Europe plate convergence and were characterized by migrating outer compressional and inner extensional domains, following the northeastward retreat of the subducting Adriatic slab (e.g. Frepoli & Amato, 1997). Nowadays, the outermost active NA blind thrust fronts are found buried below the Plio-Quaternary sedimentary sequence filling the Po Plain foredeep/foreland basin system and along the mountain front (Livani et al., 2018; Maesano et al., 2015; Maestrelli et al., 2018), whereas active extension runs along the crest of the NA mountain chain and is expressed by the regional, NE-dipping, low-angle Etrurian Fault System and related antithetic faults (Boncio et al., 2000). In this region, the causative faults of the larger earthquakes exhibit largely variable kinematics, ranging from extensional to compressional,

and have variable hypocentral depths from very shallow to deep (i.e. from 2 km of depth, up to over 30 km, see Table 2 in Sbarra et al., 2019; see also DISS Working Group, 2021; Vannoli et al., 2015). The macroseismic intensities felt in the localities surrounding the Roncovetro landslide, which can be taken as a proxy of the seismic shaking, peaks with the Modified Mercalli intensity scale (MCS) VII induced by the M_w 6.5, 1920 Garfagnana earthquake (CFTI5Med catalogue, Guidoboni et al., 2018, 2019). Conversely, the more numerous compressional earthquakes generated by the NA active thrusts, induced lower macroseismic intensities with maximum values of V-VI and VI MCS during the Mw 5.0, 1983 and Mw 5.4, 2008 Parmense earthquakes (CPTI15 catalogue, Rovida et al., 2020, 2021). The Mw 6.1, 2012 Emilia seismic sequence was only felt with an intensity of IV-V MCS (De Rubeis et al., 2019) (Figure 2).

The stratigraphic sequence outcropping in the landslide area belongs to the Ligurian and Sub-ligurian domains (Conti et al., 2020). The first unit consists of Mesozoic and early Cenozoic sedimentary successions and Jurassic ophiolites representing the remains of the Ligurian-Piedmont ocean, that from Late Cretaceous to middle Eocene was deformed and incorporated into the Alpine accretionary wedge. The second unit was deposited since the middle Eocene in wedge-top basins unconformably covering the first one (Marroni et al., 2010). Both units are intensely deformed and tectonised and are composed mainly of shaly-clayey calcareous-arenaceous flysch. In particular, in the landslide area the following geological formations outcrop: Val Samoggia Variegated Shales (highly tectonized shales), Palombini Shales (highly tectonized shales), Casanova Complex (matrix-supported monogenic breccia), Ponte Bratica Sandstones (thinly-bedded, arenitic turbidites), Canetolo Shales and Limestones (deformed shales with limestones and silty sandstone turbidites) (Figure 3).

2.2. The Roncovetro landslide

The Roncovetro landslide affects the southern flank of Monte Staffola from the crest, where its crown is located, down to the Tassobbio river where the landslide toe ends (Figure 1). It is 2.5 km long and has a total volume of $\sim 3 \times 10^6$ m^3 (Bertolini & Gorgoni, 2001). Since the clay fraction is largely dominant, the landslide mainly behaves like a fluid-viscous earth flow able to reach maximum velocities up to 10 m/day, while the landslide's head acts as a translational earth-slide (Bertolini & Gorgoni, 2001). It was first described by Almagià (1907), who reported that the detachment could have started between the middle

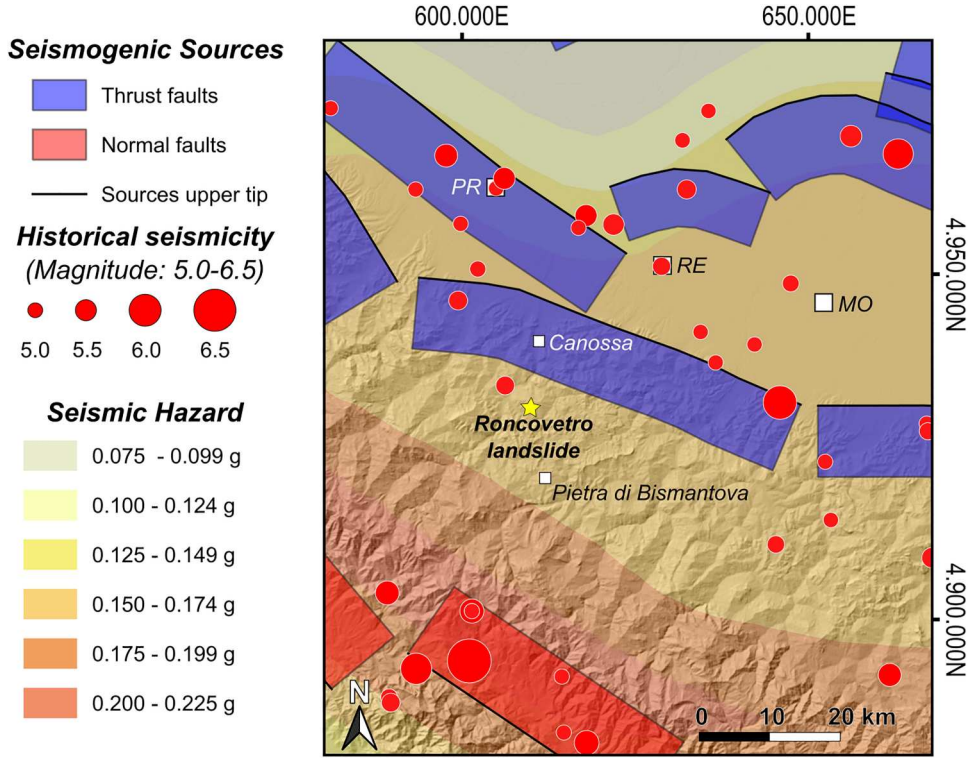

Figure 2. Seismotectonic setting of the study area showing in the background the seismic hazard map of Italy (MPS04; Stucchi et al., 2004), where the different colours show the ground acceleration with a 10% probability of exceedance in 50 years, and in the foreground the composite seismogenic sources of the DISS database (DISS Working Group, 2021) differentiated according to their kinematics. A thick black line highlights their upper tip. Historical earthquakes from the CPTI15 Catalogue with Mw > 5 are shown with red circles of area proportional to their magnitude (Rovida et al., 2020, 2021). Cities (white squares): MO: Modena, PR: Parma, RE: Reggio Emilia. Coordinates are in metres in the WGS84 UTM32N system.

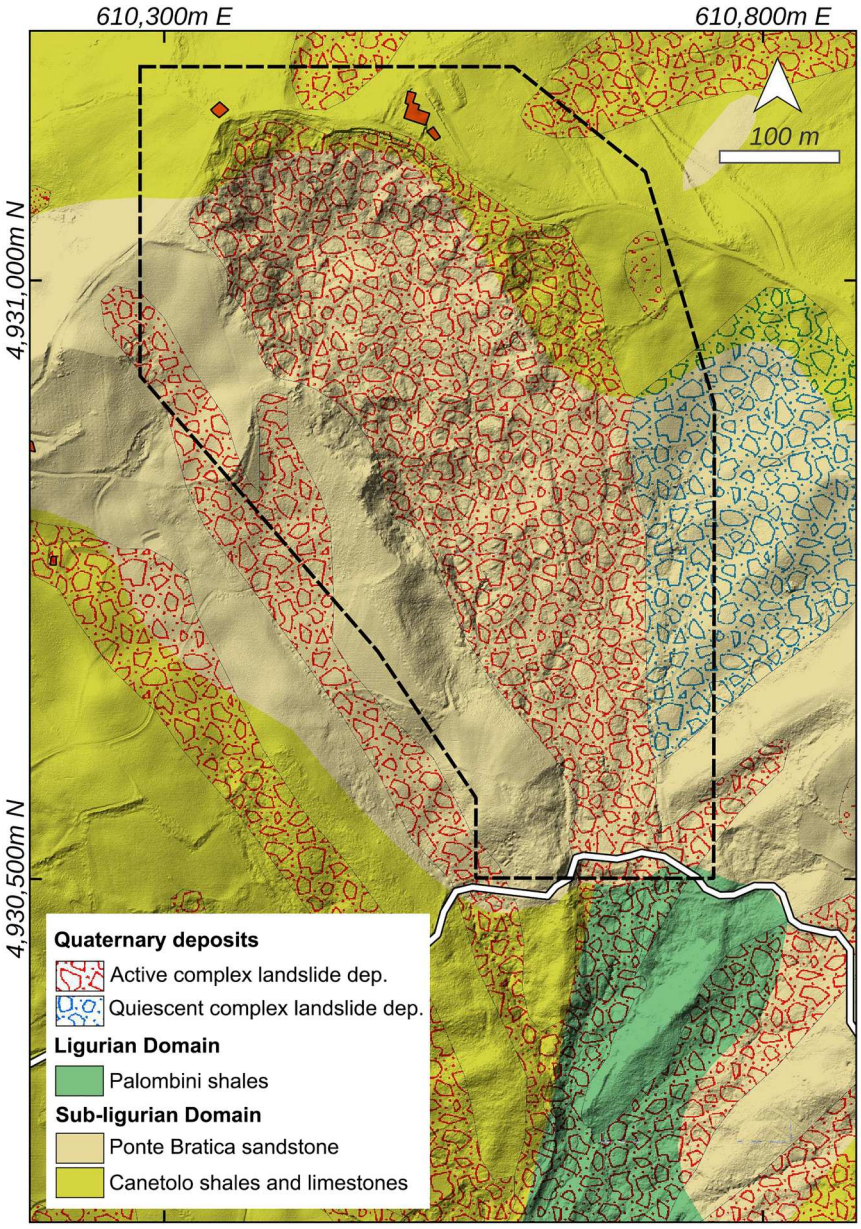

Figure 3. Geological setting of the landslide area in WGS84 UTM32 coordinate reference system. Detail of Emilia-Romagna geological map 1:10.000 (Regione Emilia Romagna Geoportale, 2020) mapped on the 2014 LiDAR DEM. The black dotted lines indicates the study area.

and the end of the XIX century. The landslide was reactivated in the early '90s and since then it had a rapid and continuous evolution, mainly characterized by the rapid retrogression of its crown to the extent that it has now reached the top of Mount Staffola (Bertolini & Fioroni, 2013; Bertolini & Gorgoni, 2001).

Bertolini and Gorgoni (2001) asserted that the continuous activity of the Roncovetro landslide is caused by high pore-water pressures maintained by the inflow of highly mineralized groundwater mixed with methane coming from the subsurface. Cervi and Tazioli (2021) add that an important recharge quota is supplied by infiltrative water from the fractures located on the top of the landslide. Although the seismic activity has never been identified as a triggering cause, like for other Emilia Apennine landslides, also for the Roncovetro landslide triggering due to earthquakes can not be excluded (Bertolini et al., 2005).

The perennial activity of the Roncovetro landslide is characterized by phases during which the detachment is limited to deep creep, sliding and flowing and major events (the last one occurred on March 2023), which cause the interruption of the white road between Roncovetro and Vedriano villages (Figure 1). Archive documents cite 10 main events between 1889 and 2002 (Bertolini, 2010). From 2014 to August 2023, we report four interruptions of the road between Roncovetro and Vedriano villages: in March 2015, May 2019 (Gracchi, 2019), December 2020 and the last one occurred on March 2023.

Based on morphological features, the landslide can be divided into three main sectors (Figure 1b): (i) the

Upper Sector (depletion zone); (ii) the Middle channel and; (iii) the Lower Sector (accumulation zone) (Bertolini & Gorgoni, 2001).

The Upper Sector (depletion zone) is the ~715 m long uppermost part of the landslide that includes the crown, the main scarp and the upper part of the landslide body (Figure 1b). It is fed by surficial mud and earth flows, coming from the main scarp, which is continuously replenished by clay and highly mineral water coming out from several springs located in the main scarp. The upper landslide body moves downslope through rotational surfaces of rupture visible also on the mountain top and beyond it (Bertolini & Gorgoni, 2001). The Middle Channel is a long (~1.26 km) and narrow channel (~30–40 m wide), deeply carved into the bedrock, that allows the earth to flow from the depletion area to the deposition area, maintaining in confined conditions its fluidity (Bertolini & Gorgoni, 2001). The Lower Sector (accumulation zone) is ~700 m long and it starts at the exit of the natural channel and ends at the Tassobbio river. Here the landslide becomes more plastic and acquire a convex shape. In this sector, the main mechanism of movement is sliding (Bertolini & Gorgoni, 2001).

In this work, we only analyse the Upper Sector of the Roncovetro landslide.

3. Material and methods

3.1. Geomorphological mapping

The geomorphological map of the Roncovetro landslide was realized by interpreting the 2014s airborne LiDAR-derived DEM, and its derivative maps (Figures 1 and 4). At the time of writing, the 2014s LiDAR DEM is still the most complete and detailed topographic data of this landslide. One of the advantages of the use of LiDAR is its capability of penetrating through the high vegetation, allowing to acquire the topographic information also where the landslide has been stable for a while and has been revegetated. In addition to LiDAR data, an orthophoto of the same period was used. All data were visualized and edited on QGIS (QGIS, 2020) for the following geomorphological mapping. Several geomorphological field surveys were also carried out for validating and integrating the analysis from remote data.

The airborne LIDAR survey was carried out on 31st October 2014. The acquired area was about 1.5 km × 3.5 km wide (Figure 1a). The total number of the acquired points was 64.8×10^6 for a point density of 14.3 points/m^2. This allowed us to produce a DEM of 20 × 20 cm of pixel size (Figure 1a). Using the 20-cm LiDAR-derived DEM, we derived variables useful for the geomorphological mapping using C++ code developed *ad-hoc* (Favalli & Fornaciai, 2017). We calculated and used the shaded relief, the slope, the sky view factor (SVF) (Steyn, 1980; Zakšek et al., 2011), and the openness down (Yokoyama et al., 2002) maps (Figure 4). The SVF variable is defined in terms of the solid angle (Ω) open to the sky and it is expressed as the sky percentage visible from any given point of the surface, i.e. SVF = $\Omega/2\pi$ (Favalli & Fornaciai, 2017). Since ridges lines and crests will be incident to nearly all of the incoming light, as consequence these features will have SVF values close to one. The opposite will be for depressed areas. Openness down (Ψ_R) are the measure of the belowground openness (Yokoyama et al., 2002). It has high values inside valleys, gullies, thalwegs, fractures and so on (Figure 4c; Favalli & Fornaciai, 2017).

The orthophoto was generated starting from a set of photos taken during an aerial survey, performed using a two seats aircraft Tecnam P92, carried out on 13 March 2014 by one of the authors (G. Bertolini). A total of 181 photos were taken over the landslide by a consumer-grade camera. Structure from Motion (SfM) methods, implemented in the Agisoft PhotoScan software version 1.2, was then used for generating the final orthophoto.

3.2. Lidar DEMs co-registration and change detection

Active landslide evolution in a given time interval is obtained by differencing the two DEMs derived from data acquired at different times. This calculation can be affected by errors due to the presence of a mismatch between two DEMs, which leads to artefact Δh (Favalli et al., 2010). This error can be detected and reduced by measuring and minimizing the DEM differences in areas where the two DEMs are supposed to be equal, i.e. those areas, external to the landslide, that were not affected by relevant natural changes.

In this work, we compare the 20 cm resolution 2014 LiDAR, described above, with the 5 m resolution DEM of the Emilia-Romagna Region (Regione Emilia Romagna Geoportale, 2020). The latter was created by using the elevation data derived from the Regional Technical Map (RTM) at the 1:5000 scale (Regione Emilia Romagna Geoportale, 2020). For the investigated area, the 5 m DEM is based on data acquired on 1973 (personal communication from RER). It follows, that the difference between the 2014 DEM and the 1973 DEM measure the mass wasting of the Roncovetro landslide due to events in 1973, 1978, 1982, 1986 and 1988 (Bertolini & Gorgoni, 2001), as well as all the displacement that occurred after the 1994 reactivations until the 2014 LiDAR survey.

DEM-to-DEM co-registration was based on the minimization of the root mean square (RMS) error between one DEM and the other (e.g. Favalli et al., 2018). We followed the same workflow described in

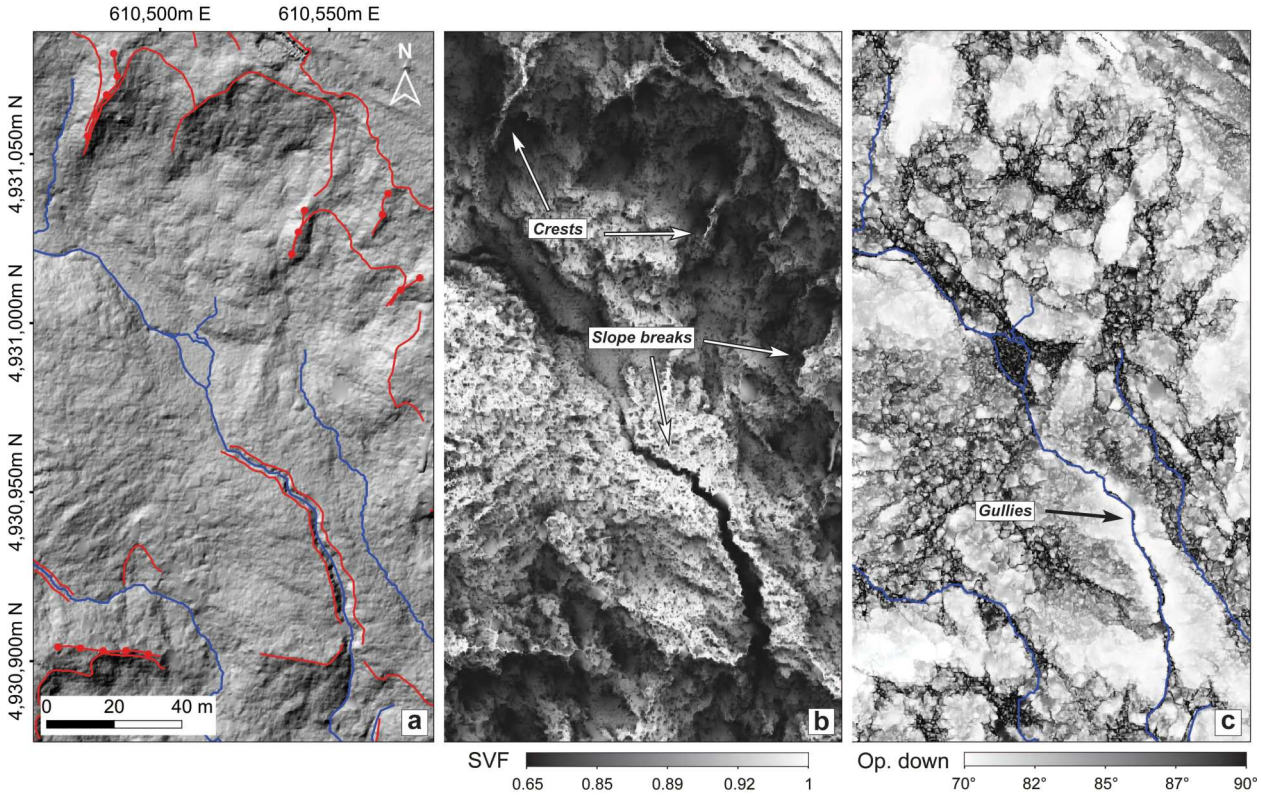

Figure 4. Extraction of the main features from a detail of the NE side of the mass movement upper part. (a) Hillshaded map with lines defining gravity- and water-related forms extracted from DEM-derived maps; (b) Sky View Factor (SVF) map, which allows identification of crest and slope breaks belonging to scarp lines and gullies erosion scarps; (c) Openness Down (Op. Down) map, which allows identification of gully thalwegs.

Di Traglia et al. (2020). After the two DEMs are co-registered, the RMS displacement error ($\sigma_{\Delta Z}$) between the 2014 LiDAR-DEM (used as reference) and the DEM of the Emilia-Romagna Region was 1.15 m. The topographic changes are shown in Figure 5. The profiles of Figure 6 show the good matching between the two DEMs.

The differences between the two co-registered DEMs were used to detect the areas that were affected by topographic changes and to calculate the volume and thickness variation inside them (Figures 5 and 6). The volume (V) added or lost between two acquisitions was calculated from the DEM difference according to $V = \Sigma_i \Delta x^2 \Delta z_i$ (Favalli et al., 2010), where Δx is the grid step and Δz_i is the height variation within the grid cell i. These values were then summed for all the cells in the selected areas in which the volume changes were calculated. An upper bound on the error for the volume estimate was given by assigning to each pixel the maximum possible error, i.e. $Err_{V,high} = A\sigma_{\Delta Z}$, where A is the investigated area (Favalli et al., 2010).

4. Results and discussion

The upper sector of the Lavina di Roncovetro landslide is about 715 m long, elongated in the NW-SE direction. Landslide morphology is strongly influenced by its fluid-like behaviour, mainly due to the involvement of tectonised clay-dominant formations with the contribution of the water recharge from within the slope (Bertolini & Gorgoni, 2001; Cervi & Tazioli, 2021). The main geomorphological features were identified according to 2014s morphogenetic environmental setting. They were mapped within the landslide and were defined as follows.

The gravity-induced landforms and deposits included: (i) the crown: high-angle slope break bounding the highest parts of the main scarp; (ii) the crown crack: the shear fissure affecting the ground beyond the crown; (iii) the scarp line: the slope break delimiting minor gravitational processes; (iv) the crest: top of a ridge, a flank ridge or a pressure ridge; (v) the transverse crack; (vi) the counter-slope: the surface dipping in the counter direction in relation to the landslide main movement direction; (vii) the rock slide: downslope movement of a mass of rock along a distinctive rupture or slip surface; (viii) the main scarp: the steep surface at the upper edge of the landslide created when the movement of the displaced material exposes a part of the surface of rupture, it represents the zone of depletion; (ix) the earth flow: a viscous flow of fine-grained materials that have been saturated with water and moves under the pull of gravity; and (x) the

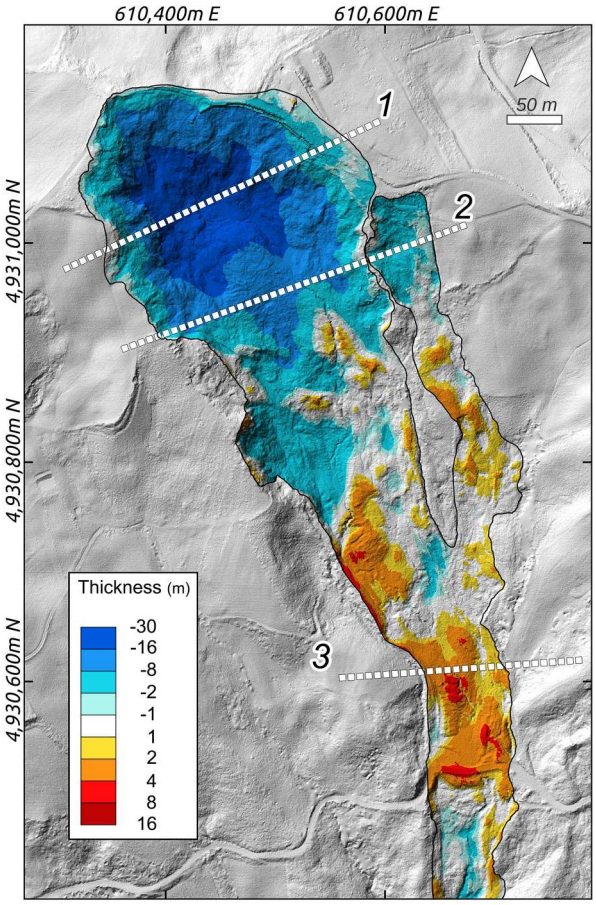

Figure 5. Topographic change detection showing the volume lost and accumulated in about 40 years before the 2014 LiDAR survey. The location of the profiles of Figure 6 are shown. Coordinates are in the WGS84 UTM32 system.

landslide flank: the undisplaced material adjacent to the sides of the rupture surface.

The fluvial and runoff landforms and deposits included: (i) the rill: the shallow and narrow channel created by surface runoff; (ii) the gully: the deeper and larger channel created by concentrated surface runoff; (iii) the erosional scarp: the slope break bounding the upper edge of the channel bank; (iv) the crest: the top of a fluvial ridge; (v) the alluvial fan: the outspread sloping mass of loose material deposited by a stream that issues from a narrow canyon onto a plain or valley floor; and (vi) the pond.

The anthropogenic structures included: (i) the crib wall: the retaining structures to improve the slope stability, (ii) the building; and (iii) the road.

The study area shows a complex system of different movement mechanisms.

The region that includes the rock slide, the main scarp, the crown and the zone of crown cracks, extending from the top of the slope (~ 693 m a.s.l.) down to ~ 630 m a.s.l., is affected by a roto-translational movement. The zone of crown cracks marks the upslope boundary of the area affected by the mass movement. The tension cracks are visible in both field and remote surveys. They indicate the regressive behaviour of the sliding movement that on the NE side expands beyond the upper road up to the building. This area is characterized by the presence of rotational surfaces of rupture that affect the Sub-Ligurian formations. Over the years, the movement of this deformation area has been demonstrated by two inclinometers, installed by the RER, that detected the slip surface at about 10–12 m of depth. Gravity-related landforms and shallow secondary flows, which are continuously fed by highly mineralized water emerging from the springs located in this area (Bertolini & Gorgoni, 2001), are also present. The presence of mineralized water (Bertolini & Gorgoni, 2001; Cervi & Tazioli, 2021) is highlighted by thick whitish crusts deposited over the main scarp area (Figure 7a). Surface runoff processes, mainly related to shallow and narrow channels, also model this area and affect the secondary landslides contributing to material erosion (Figure 7a). An abrupt break in slope at 630 m a.s.l. marks the beginning of an gently sloped area with a mean slope of 16.5°. Rills and gullies cut through the body resulting in ponds and alluvial fan deposits. Moreover, gully, crests and escarpments are identifiable. This area is also characterized by an elongated hummocky shape resulting from an extensional-compressional regime of the sliding movement. The hummock area is bordered by several water ponds and gully tracks (Figure 7a).

At ~ 630 m a.s.l. the body develops in counter-slopes and steep scarps showing the body's internal deformation produced by shear surfaces (Bertolini & Fioroni, 2013). This marks the beginning of the landslide channel, soon after the two landslide flanks are visible. The eastern flank is interrupted at ~ 570 m a.s.l. by a secondary branch of the landslide that flows in the main slide just above the white road (Figure 7b). A gully creek tracked from water erosion longitudinally engraves the material and forms an alluvial fan. A main deep gully flanks this area and crosses the whole upper part of the main body connecting with several ponds. Slightly above the white road, the main gully results in an alluvial fan (between ~ 562 and ~564 m a.s.l.) that has a maximum width of around 37 m and a length of around 40 m (Figure 7b). Downslope from the area marked by counter-slopes previously mentioned, younger and older flow deposits twist and turn forming lobes and ridges modelled by water-erosion processes.

The mass movement boundary is associated with two lateral ridges, on the right and left flanks. The other two crests internally bound the landslide. These flow-characteristic landforms are indicators of the movement rate (Bertolini & Fioroni, 2013; Guerriero et al., 2014; Parise, 2003); in this case, the external ridges are older than the internal ones showing a

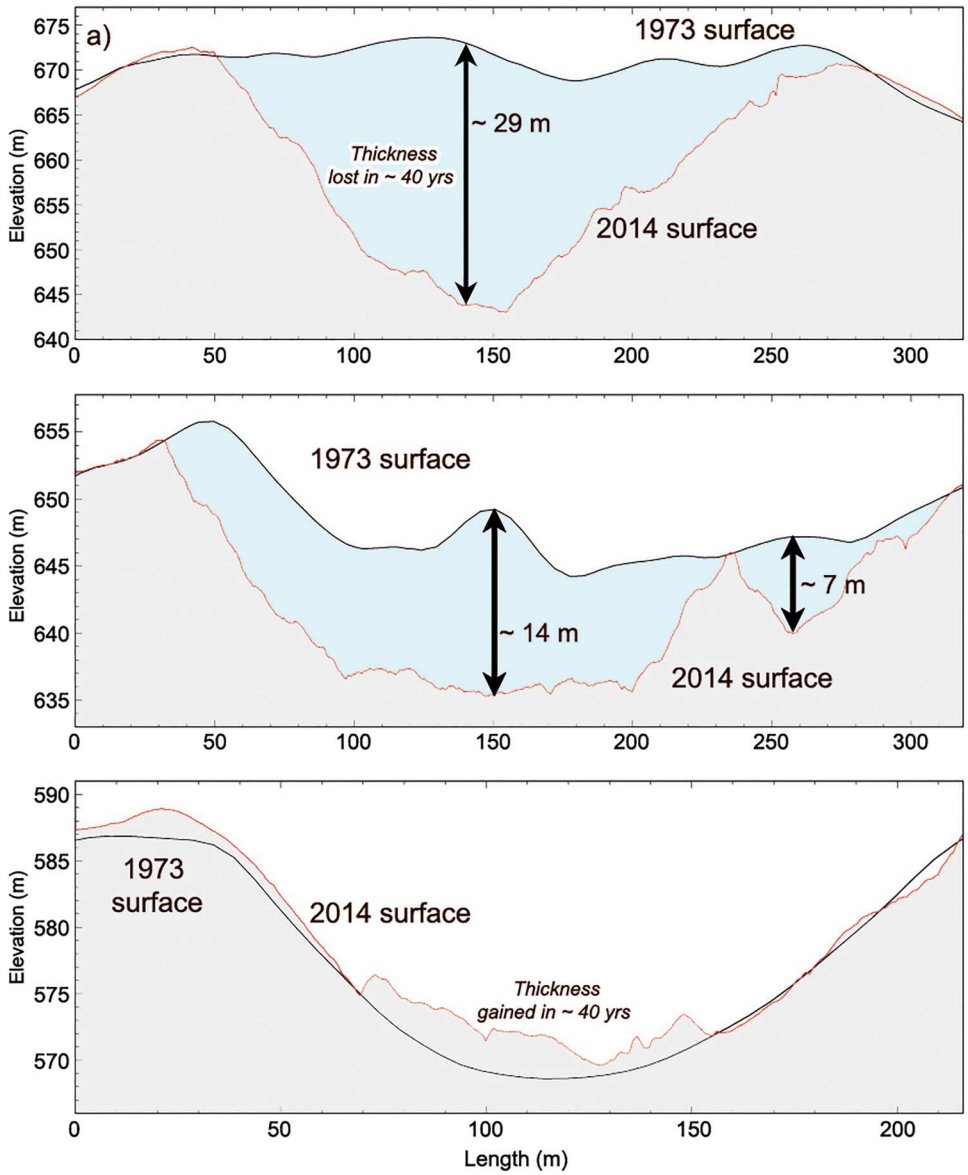

Figure 6. Selected profiles that show two sections of the volume-loss area (a and b) and one section where the volume accumulated (c).

decrease in the landslide's width and therefore a reduction of the flowing material.

Comparison between RER and 2014 LiDAR DEMs (Figures 5 and 6) shows that in about 40 years, the S flank of Monte Staffola has been massively carved out by the landslide. The volume moved from the top, only partially accumulating before the white road. About $6.2 \pm 0.8 \times 10^5$ m^3 of material moved from the top towards the lower sector of the landslide. The average thickness of volume loss was 9.4 ± 1.2 m, with the maximum value reaching –29 m (Figure 6, profile 1). The mean discharged rate is therefore ~ 0.16×10^5 m^3/yr. The volume accumulated before the white road is about 0.4×10^5 m^3, which means that most of the discharged material moved towards the middle channel and the toe. The average thickness of the volume accumulated was 2.2 ± 1.2 m. Also, the eastern branch of the slide has been affected by mass wasting in the considered period.

5. Conclusions

The Main Map created in this work describes the geomorphological status of the upper sector of the Roncovetro Landslide in October 2014. Despite the continuous activity of the landslide, the capability of LiDAR to pass through the vegetation makes the 2014 data still the most complete and accurate topographic dataset of this landslide, which allows us to detect also the quiescent areas covered by the vegetation.

The main geomorphological map of the upper portion of the Roncovetro landslide was realized in 1:1500 scale by the interpretation of airborne LiDAR-derived DEM and its derivative maps, by the orthophoto built using the 2014 aerial photos and the SfM method, and by periodical field surveys. The map can be useful for future projects that could find this area as a suitable site for testing experimental technologies for landslide monitoring.

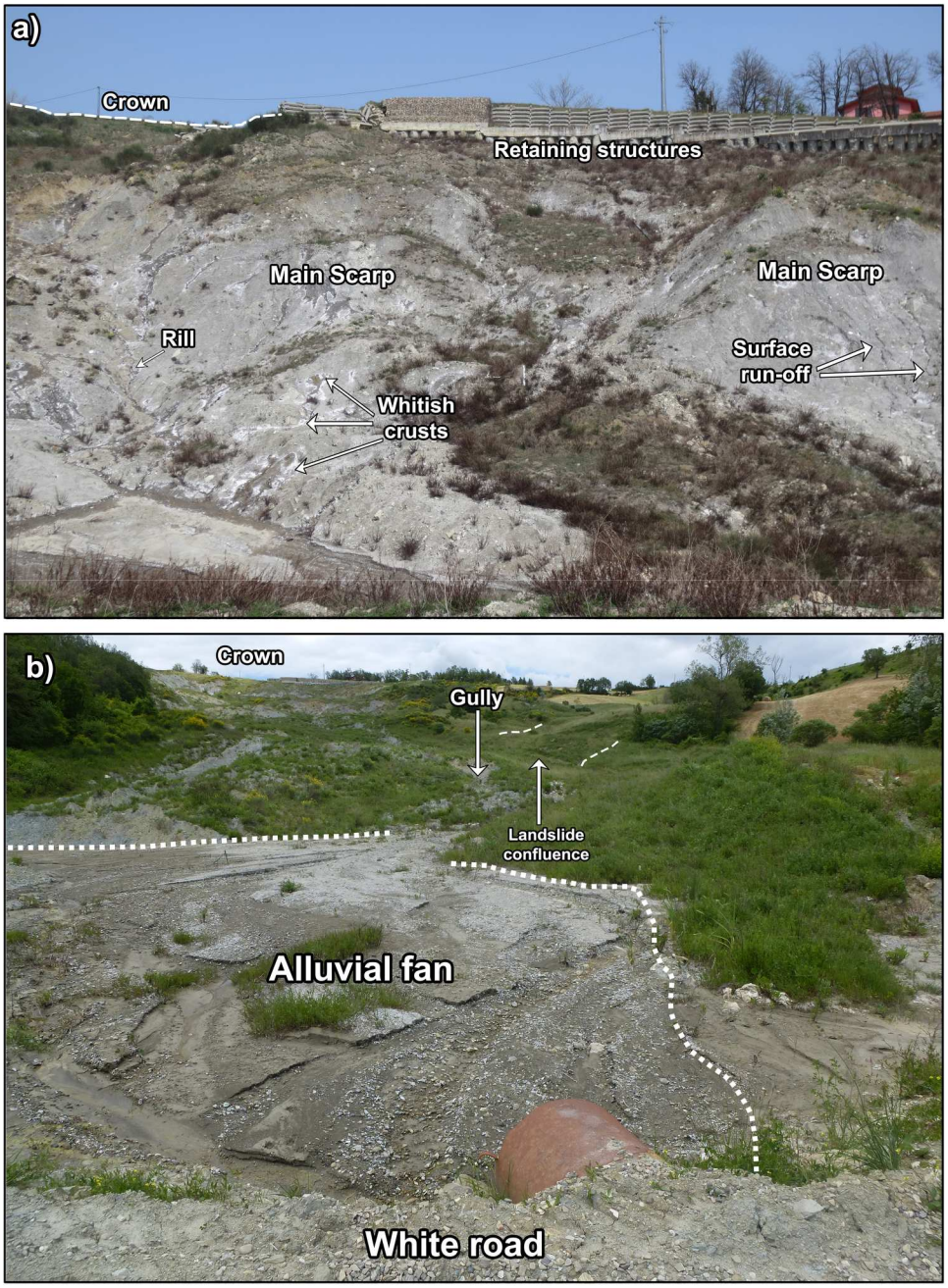

Figure 7. (a) Photo of a part of the main scarp area taken on 06 April 2016 from the bottom upward. Relevant features are highlighted; (b) photo of the upper sector of Roncovetro landslide taken on 28 May 2014 from the white road with the alluvial fan at the end of one of the main gully in foreground. The approximate position from which the photos were taken is indicated in Figure 1(c).

The general morphology of the Roncovetro landslide is influenced by the kinematic mechanisms involved, i.e. sliding and flowing, and by the water content of the material and, consequently, by its state of fluidity. Sliding failure on rotational surfaces affects the upper limit of the mass movement, where its regressive behaviour is evident by remote and field surveys. It is the initiating mechanism of earth flow major events. The identified features linked to gravity, such as cracks, scarps, crests, and counter-slopes, are the result of these main processes and secondary short-term landslides. Furthermore, the gravity-induced surfaces and deposits are remodelled by water runoff resulting in erosional (i.e. rills, gullies, erosional scarps and crests) and depositional (alluvial fans) forms.

The Roncovetro landslide was reactivated entirely in the early '90s and since then it has been in a perennial state of activity. The main cause of its movement is supposed to be the inflow of highly mineralized waters from the subsoil (Bertolini & Gorgoni, 2001). By comparing the RER's DEM and the 2014 LiDAR DEM we calculated that a volume of $6.2 \pm 0.8 \times 10^5$ m^3 has been carved out from the south flank of Monte Staffola in about 40 years.

Software

The final map was edited using the software QGIS (QGIS, 2020, v. 2.18.17, Las Palmas) and refined with Adobe Illustrator® CS6 16.0.0. The map legend was inspired by the guidelines of the Geomorphological Map of Italy (Servizio Geologico Nazionale, 1994) and adapted for this work as dictated by landforms present on the Roncovetro landslide.

Disclosure statement

No potential conflict of interest was reported by the author(s).

Funding

This research was partially supported by the project 'Wi-GIM: Wireless sensor network for Ground Instability Monitoring' financed by the Life + EU Program (LIFE12/ENV/IT001033), by the project 'Integrated and multi-scale approach for the definition of earthquake-induced landslide hazard in the Italian territory' funded by the Italian Ministry of Environment, Land and Sea and by the 'Landslide Enhanced MOnitoring Network' project funded by the Istituto Nazionale di Geofisica e Vulcanologia.

References

Almagià, R. (1907). Studi geografici sopra le frane in Italia. *Mem. Soc. Geogr. It.*, *13*(1), 342.

Bertolini, G. (2010). Large earth flows in Emilia-Romagna (northern Apennines, Italy): origin, reactivation and possible hazard assessment strategies. *Zeitschrift der Deutschen Gesellschaft für Geowissenschaften*, *161*(2), 139–162. https://doi.org/10.1127/1860-1804/2010/0161-0139

Bertolini, G., & Fioroni, C. (2013). Large reactivated earth flows in the northern Apennines (Italy): An overview. *Landslide Science and Practice: Volume 4: Global Environmental Change*, *4*, 51–58. https://doi.org/10.1007/978-3-642-31337-0_6

Bertolini, G., & Gorgoni, C. (2001). La lavina di Roncovetro (Vedriano, Comune di Canossa, Provincia di Reggio Emilia). *Quad. Geol. Appl.*, *8*(2), 1–23.

Bertolini, G., Guida, M., & Pizziolo, M. (2005). Landslides in Emilia-Romagna region (Italy): strategies for hazard assessment and risk management. *Landslides*, *2*(4), 302–312. https://doi.org/10.1007/s10346-005-0020-1

Boncio, P., Brozzetti, F., & Lavecchia, G. (2000). Architecture and seismotectonics of a regional low-angle normal fault zone in central Italy. *Tectonics*, *19*(6), 1038–1055. https://doi.org/10.1029/2000TC900023

Cervi, F., & Tazioli, A. (2021). Coupling mineralogical analyses, leaching tests and kinetic modelling to unravel groundwater flow-paths in a complex landslide: An attempt from the vedriano case study (northern Italian Apennines). *Geosciences*, *11*(1), 1. https://doi.org/10.3390/geosciences11010001

Conti, P., Cornamusini, G., & Carmignani, L. (2020). An outline of the geology of the northern Apennines (Italy), with geological map at 1: 250,000 scale. *Italian Journal of Geosciences*, *139*(2), 149–194. https://doi.org/10.3301/IJG.2019.25

Cruden, D. M., & Varnes, D. J. (1996). Landslide types and processes. In A. K. Turner, & R. L. Schuster (Eds.), *Landslides: Investigation and mitigation* (pp. 36–75). National Academy Press.

De Rubeis, V., Sbarra, P., Tosi, P., & Sorrentino, D. (2019). Hai Sentito Il Terremoto (HSIT) - Macroseismic intensity database 2007-2018, version 1.

DISS Working Group. (2021). Database of Individual Seismogenic Sources (DISS), Version 3.3.0: A compilation of potential sources for earthquakes larger than M 5.5 in Italy and surrounding areas. Istituto Nazionale di Geofisica e Vulcanologia (INGV). https://doi.org/10.13127/diss3.3.0

Di Traglia, F., Fornaciai, A., Favalli, M., Nolesini, T., & Casagli, N. (2020). Catching geomorphological response to volcanic activity on steep slope volcanoes using multi-platform remote sensing. *Remote Sensing*, *12*(3), 438. https://doi.org/10.3390/rs12030438

Favalli, M., & Fornaciai, A. (2017). Visualization and comparison of DEM-derived parameters. *Application to Volcanic Areas. Geomorphology*, *290*, 69–84.

Favalli, M., Fornaciai, A., Mazzarini, F., Harris, A., Neri, M., Behncke, B., Pareschi, M. T., Tarquini, S., & Boschi, E. (2010). Evolution of an active lava flow field using a multitemporal LIDAR acquisition. *Journal of Geophysical Research: Solid Earth*, *115*(B11), B11203. https://doi.org/10.1029/2010JB007463

Favalli, M., Fornaciai, A., Nannipieri, L., Harris, A., Calvari, S., & Lormand, C. (2018). UAV-based remote sensing surveys of lava flow fields: A case study from etna's 1974 channel-fed lava flows. *Bulletin of Volcanology*, *80*(3), 1–18. https://doi.org/10.1007/s00445-018-1192-6

Frepoli, A., & Amato, A. (1997). Contemporaneous extension and compression in the northern Apennines from earthquake fault-plane solutions. *Geophysical Journal International*, *129*(2), 368–388. https://doi.org/10.1111/j.1365-246X.1997.tb01589.x

Gracchi, T. (2019). *Wireless sensor networks for landslide monitoring: application and optimization by visibility analysis on 3D point clouds* [Doctoral dissertation, University of Florence].

Guerriero, L., Coe, J. A., Revellino, P., Grelle, G., Pinto, F., & Guadagno, F. M. (2014). Influence of slip-surface geometry on earth-flow deformation, Montaguto earth flow, southern Italy. *Geomorphology*, *219*, 285–305. https://doi.org/10.1016/j.geomorph.2014.04.039

Guidoboni, E., Ferrari, G., Mariotti, D., Comastri, A., Tarabusi, G., Sgattoni, G., & Valensise, G. (2018). CFTI5Med, catalogo dei Forti Terremoti in Italia (461 a.C.-1997) e nell'area Mediterranea (760 a.C.-1500). *Istituto Nazionale di Geofisica e Vulcanologia*. https://doi.org/10.6092/ingv.it-cfti5

Guidoboni, E., Ferrari, G., Tarabusi, G., Sgattoni, G., Comastri, A., Mariotti, D., Ciuccarelli, C., Bianchi, M. G., & Valensise, G. (2019). CFTI5Med, the new release of the catalogue of strong earthquakes in Italy and in the Mediterranean area. *Scientific Data*, *6*(1), 1–15. https://doi.org/10.1038/s41597-019-0091-9

Intrieri, E., Gigli, G., Gracchi, T., Nocentini, M., Lombardi, L., Mugnai, F., Frodella, W., Bertolini, G., Carnevale, E., Favalli, M., Fornaciai, A., Alavedra, J. M., Mucchi, L., Nannipieri, L., Lloveras, X. R., Pizziolo, M., Schina, R., Trippi, F., & Casagli, N. (2018). Application of an ultra-wide band sensor-free wireless network for ground monitoring. *Engineering Geology*, *238*, 1–14. https://doi.org/10.1016/j.enggeo.2018.02.017

Livani, M., Scrocca, D., Arecco, P., & Doglioni, C. (2018). Structural and stratigraphic control on salient and recess development along a thrust belt front: The northern Apennines (Po plain, Italy). *Journal of Geophysical Research: Solid Earth*, *123*(5), 4360–4387. https://doi.org/10.1002/2017JB015235

Maesano, F. E., D'Ambrogi, C., Burrato, P., & Toscani, G. (2015). Slip-rates of blind thrusts in slow deforming areas: Examples from the Po plain (Italy). *Tectonophysics*, *643*, 8–25. https://doi.org/10.1016/j.tecto.2014.12.007

Maestrelli, D., Benvenuti, M., Bonini, M., Carnicelli, S., Piccardi, L., & Sani, F. (2018). The structural hinge of a chain-foreland basin: Quaternary activity of the pede-apennine thrust front (northern Italy). *Tectonophysics*, *723*, 117–135. https://doi.org/10.1016/j.tecto.2017.12.006

Marroni, M., Meneghini, F., & Pandolfi, L. (2010). Anatomy of the Ligure-Piemontese subduction system: evidence from Late Cretaceous–middle Eocene convergent margin deposits in the Northern Apennines, Italy. *International Geology Review*, *52*(10–12), 1160–1192. https://doi.org/10.1080/00206810903545493

Mucchi, L., Jayousi, S., Martinelli, A., Caputo, S., Intrieri, E., Gigli, G., Gracchi, T., Mugnai, F., Favalli, M., & Fornaciai, A. (2018). A flexible wireless sensor network based on ultra-wide band technology for ground instabil-ity monitor-ing. *Sensors*, *18*(9), 2948. https://doi.org/10.3390/s18092948

Parise, M. (2003). Observation of surface features on an active landslide, and implications for understanding its history of movement. *Natural Hazards and Earth System Sciences*, *3*(6), 569–580. https://doi.org/10.5194/nhess-3-569-2003

QGIS Development Team. QGIS geographic information system. Retrieved September 2020. http://qgis.osgeo.org

Regione Emilia-Romagna Geoportale. (2020). DTM 5 (5. Retrieved February 2022. https://geoportale.regione.emilia-romagna.it/catalogo/daticartografici/altimetria/layer-2

Rovida, A., Locati, M., Camassi, R., Lolli, B., & Gasperini, P. (2020). The Italian earthquake catalogue CPTI15. *Bulletin of Earthquake Engineering*, *18*(7), 2953–2984. https://doi.org/10.1007/s10518-020-00818-y

Rovida, A., Locati, M., Camassi, R., Lolli, B., Gasperini, P., & Antonucci, A. (2021). Catalogo Parametrico dei Terremoti Italiani (CPTI15), versione 3.0. *Istituto Nazionale di Geofisica e Vulcanologia (INGV)*.

Sbarra, P., Burrato, P., Tosi, P., Vannoli, P., De Rubeis, V., & Valensise, G. (2019). Inferring the depth of pre-instrumental earthquakes from macroseismic intensity data: A case-history from northern Italy. *Scientific Reports*, *9*(1), 1–13. https://doi.org/10.1038/s41598-019-51966-4

Servizio Geologico Nazionale. (1994). Carta Geomorfologica d'Italia 1:50.000. Guida al rilevamento. Quaderni, serie III, vol. 4, 42 pp., Roma, Italy.

Steyn, D. (1980). The calculation of view factors from fisheye-lens photographs. *Atmosphere-Ocean*, *18*(3), 254–258. https://doi.org/10.1080/07055900.1980.9649091

Stucchi, M., Meletti, C., Montaldo, V., Akinci, A., Faccioli, E., Gasperini, P., Malagnini, L., & Valensise, G. (2004). *Pericolosità sismica di riferimento per il territorio nazionale MPS04* [Data set]. Istituto Nazionale di Geofisica e Vulcanologia (INGV). https://doi.org/10.13127/sh/mps04/ag

Tarquini, S., Vinci, S., Favalli, M., Doumaz, F., Fornaciai, A., & Nannipieri, L. (2012). Release of a 10-m-resolution DEM for the Italian territory: Comparison with global-coverage DEMs and anaglyph-mode exploration via the web. *Computers & Geosciences*, *38*(1), 168–170. https://doi.org/10.1016/j.cageo.2011.04.018

Vannoli, P., Burrato, P., & Valensise, G. (2015). The seismotectonics of the Po plain (northern Italy): Tectonic diversity in a blind faulting domain. *Pure and Applied Geophysics*, *172*(5), 1105–1142. https://doi.org/10.1007/s00024-014-0873-0

Yokoyama, R., Shirasawa, M., & Pike, R. J. (2002). Visualizing topography by openness: A new application of image processing to digital elevation models. *Photogrammetric Engineering and Remote Sensing*, *68*(3), 257–266.

Zakšek, K., Oštir, K., & Kokalj, Ž. (2011). Sky-viewfactor as a relief visualization technique. *Remote Sensing*, *3*(2), 398–415. https://doi.org/10.3390/rs3020398